COLD SPRING HARBOR
Molecular Case Studies

RESEARCH ARTICLE

Autosomal recessive LRP1-related syndrome featuring cardiopulmonary dysfunction, bone dysmorphology, and corneal clouding

Paul R. Mark,[1,2] Stephen A. Murray,[3] Tao Yang,[4] Alexandra Eby,[2,5] Angela Lai,[6] Di Lu,[4] Jacob Zieba,[2,7] Surender Rajasekaran,[2,8] Elizabeth A. VanSickle,[1] Linda Z. Rossetti,[1,2] Lucia Guidugli,[9] Kelly Watkins,[9] Meredith S. Wright,[9] Caleb P. Bupp,[1,2] and Jeremy W. Prokop[2,7,10]

[1]Division of Medical Genetics, Spectrum Health, Grand Rapids, Michigan 49503, USA; [2]Department of Pediatrics and Human Development, College of Human Medicine, Michigan State University, Grand Rapids, Michigan 49503, USA; [3]The Jackson Laboratory, Bar Harbor, Maine 04609, USA; [4]Department of Cell Biology, Van Andel Institute, Grand Rapids, Michigan 49503, USA; [5]Department of Science, Davenport University, Grand Rapids, Michigan 49512, USA; [6]Neonatal Intensive Care Unit, Bronson Methodist Hospital, Kalamazoo, Michigan 49007, USA; [7]Genetics and Genome Sciences Program, Michigan State University, East Lansing, Michigan 48824, USA; [8]Office of Research, Spectrum Health, Grand Rapids, Michigan 49503, USA; [9]Rady Children's Institute for Genomic Medicine, San Diego, California 92123, USA; [10]Department of Pharmacology and Toxicology, Michigan State University, East Lansing, Michigan 48824, USA

Corresponding authors:
paul.mark@spectrumhealth.org;
jprokop54@gmail.com

Abstract We provide the first study of two siblings with a novel autosomal recessive LRP1-related syndrome identified by rapid genome sequencing and overlapping multiple genetic models. The patients presented with respiratory distress, congenital heart defects, hypotonia, dysmorphology, and unique findings, including corneal clouding and ascites. Both siblings had compound heterozygous damaging variants, c.11420G > C (p.Cys3807Ser) and c.12407T > G (p.Val4136Gly) in *LRP1*, in which segregation analysis helped dismiss additional variants of interest. *LRP1* analysis using multiple human/mouse data sets reveals a correlation to patient phenotypes of Peters plus syndrome with additional severe cardiomyopathy and blood vessel development complications linked to neural crest cells.

[Supplemental material is available for this article.]

Ontology terms: episodic respiratory distress; fetal ascites; hypertelorism; mild fetal ventriculomegaly; patent ductus arteriosus after premature birth; polyhydramnios; postductal coarctation of the aorta; small anterior fontanelle

Published by Cold Spring Harbor Laboratory Press

doi:10.1101/mcs.a006169

INTRODUCTION

Identifying gene variants involved in early development has been challenging because of lethality, high number of potential variants, and slow turnaround time of clinical sequencing. Mainly driven by the Rady Children's Institute for Genomic Medicine, with a record of 16.5 h from sample collection to diagnosis using genome sequencing (GS) (Owen et al. 2021), rapid genomics is becoming a central tool in diagnosis within early childhood. Rapid GS (rGS) effectively impacts clinical care for pediatric patients in real time, specifically in the areas of medical and surgical management, palliative care, connecting patients with research opportunities, and family planning (Farnaes et al. 2018). Of the first 24 patients investigated with rGS by our site (Helen DeVos Children's Hospital), six were classified as having variants of

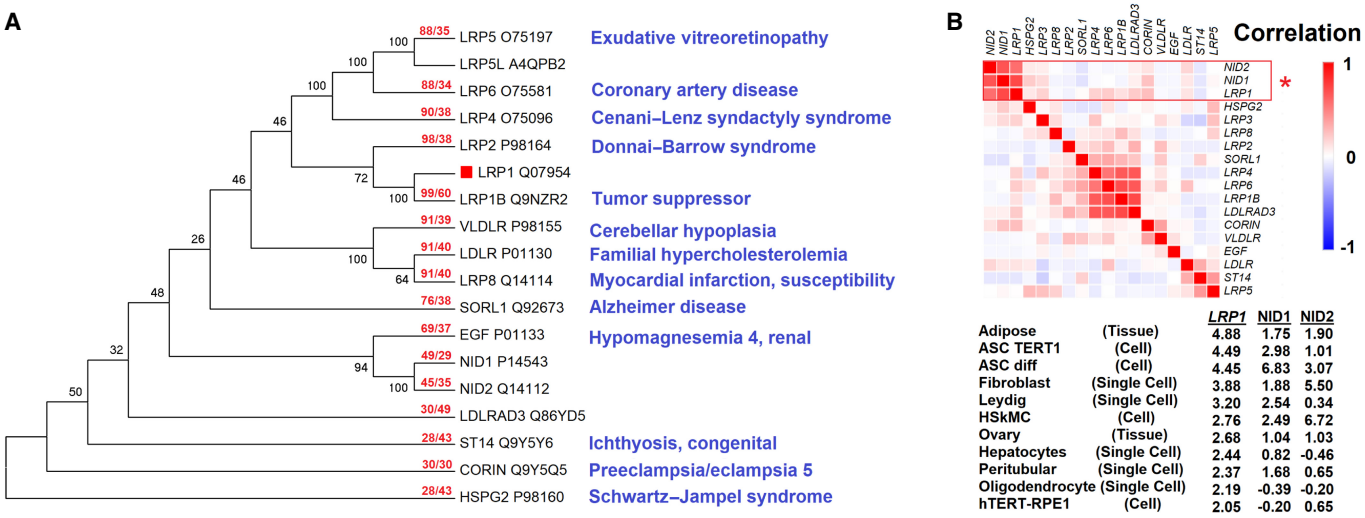

Figure 1. The low-density lipoprotein (LDL) receptor family and development. (*A*) Sequences with an E-value $<1 \times 10^{-20}$ based on BLAST of human LRP1 protein (red box). Sequences were aligned with the MUSCLE algorithm. The maximum likelihood tree shows the percent of 100 bootstrap analyses clustering at each node. The red text for each protein shows the length of coverage in BLAST hit followed by the percent identity relative to LRP1. Blue text is based on OMIM-annotated diseases for each gene. (*B*) Expression matrix for the genes of panel *A* using 200 data sets of tissues, cell lines, and single-cell annotations of the Human Protein Atlas. Correlations were calculated as 1 – Pearson's correlation. Below are the top samples for *z*-scores of LRP1, NID1, or NID2 expression levels.

uncertain significance (VUSs) (Beuschel et al. 2021), suggesting a higher percentage of uncertain classification than GS testing for undiagnosed disease analysis in older children (Bick et al. 2017). As rGS is used more frequently and broadly, this has increased the number of variants in genes not previously associated with human syndromes. In many cases, genes discovered have strong overlapping phenotypes studied within the animal modeling community (Prokop et al. 2018). This article presents two siblings with compound heterozygous *LRP1* variants identified by rGS that correlated to the observations of *Lrp1* knockout in the mouse. Although LRP1 has been linked to human disease such as Alzheimer's, as of 2022, *LRP1* has not been linked to a human syndrome.

The low-density lipoprotein receptor ligated protein 1 (*LRP1*) is a low-density lipoprotein (LDL) receptor homologous to other genes like *VLDLR*, *LDLR*, and *SORL1* (Fig. 1A). Many LRP-related genes have previously been connected to severe syndromes, including *LRP2* in Donnai–Barrow syndrome (OMIM 222448), featuring facial/ocular anomalies, hearing loss, myopia, and proteinuria with kidney disfunction (Donnai and Barrow 1993); *LRP4* in Cenani–Lenz syndactyly syndrome (OMIM #212780), featuring limb and kidney alterations (Li et al. 2010); and *LRP5* in exudative vitreoretinopathy (OMIM #*603506) and osteoporosis–pseudoglioma syndrome (OMIM #259770), featuring altered osteoblast bone development and eye complications (Gong et al. 2001). Numerous LRP-related proteins have been shown to serve as receptors for Wnt signaling (Cong et al. 2004; Cadigan and Liu 2006; Li et al. 2010), including LRP1 (Terrand et al. 2009), establishing a central role of the LRP proteins in developmental biology. Although *LRP1* is connected to many genes/proteins involved in disease biology and syndromes (Supplemental Fig. S1), no studies in humans have connected *LRP1* to a syndrome. Relative to LRP-related genes, expression profiles cluster *LRP1* near *NID1* and *NID2* (Fig. 1B); all three have no annotated developmental syndrome. Within this work, we present two siblings with matching phenotypes, in which the phenotypes for *LRP1* are supported by human or mouse data.

RESULTS

Patient Phenotypes

The proband was a female born to a 31-yr-old, mother of European ancestry at 36 wk by repeat cesarean section after preterm premature rupture of membranes. Pregnancy was complicated by obesity, bipolar disorder, and insulin-dependent type-I diabetes. Prenatal ultrasounds showed ascites, cerebral ventriculomegaly, and polyhydramnios. These were confirmed by fetal magnetic resonance imaging (MRI) at 33 wk gestation. Prenatal karyotype and microarray performed on amniotic fluid were negative. Apgar scores (status of the newborn infant) were 5 (1 min) and 7 (5 min after birth), suggesting slight abnormality. Her birth weight was 3.24 kg (33rd centile), length was 47 cm (16th centile), and head circumference was 31 cm (<1st centile).

At birth, a cleft soft palate, hypertelorism, upslanting palpebral fissures, cloudy corneas, distended abdomen, paddle-shaped fingers, single palmar creases, and hypotonia were noted. She was placed on continuous positive airway pressure (CPAP) in the delivery room and progressed to intubation and eventual tracheostomy for respiratory distress and chronic lung disease. Initial echocardiogram revealed hypoplastic aortic valve, mild coarctation of the aorta, large patent ductus arteriosus, patent foramen ovale, and dysplastic pulmonary valve. Her condition progressed to pulmonary hypertension and severe hypertrophic cardiomyopathy. Brain MRI revealed mild third and lateral ventriculomegaly with a possible Dandy–Walker variant. She had stable hepatomegaly with ascites on abdominal ultrasound, with clinical resolution of ascites over time. Ophthalmology was consulted for her cloudy corneas, and she was diagnosed for bilateral glaucoma. Facial morphology was noted with palpebral fissures and enlarged pupils/irises (Fig. 2A), whereas hands were noted for paddle-shaped fingertips (Fig. 2B). She died at five months of age secondary to cardiac arrest. A time line of the clinical course is provided in Figure 2C.

The younger male sibling of the proband was born at 33 wk, 1 d (mother at 33-yr-old) via cesarean section because of decreased fetal movement and fetal bradycardia. Prenatal ultrasounds were notable for fetal abdominal ascites, bilateral cerebral ventriculomegaly, flat facial profile with a square-shaped forehead, and two-vessel umbilical cord. Polyhydramnios was present at 22 + 6 wk ultrasound consistent with nonimmune hydrops; amniotic fluid volume was normal by 33-wk scan. Genetic testing was deferred until after delivery per parents' request. The mother presented at 33 wk gestation with decreased fetal movement for 3 d, a nonreactive nonstress test (NST), and fetal bradycardia prompting emergent cesarean section under general anesthesia. The baby was initially born with no respiratory effort. He required positive pressure ventilation (PPV), cardiopulmonary resuscitation (including three doses of epinephrine), paracentesis, intubation, and surfactant administration in the delivery room. Apgar scores were 0, 0, 3 at 1, 5, and 10 min, respectively, suggesting a poor birth condition. Birthweight was 2.610 kg (94th centile), length 44 cm (59th centile), head circumference 31.7cm (83rd centile) for gestational age. At birth, he was noted to be large for gestational age with a generously sized anterior fontanelle, bilateral corneal opacities, low-set ears, abdominal ascites, single umbilical artery, undescended and nonpalpable bilateral testes, possible rocker-bottom feet, global hypotonia, and no spontaneous movement.

Because of respiratory failure, he was placed on mechanical ventilation. Ventilation was significantly hindered by severe restriction of lung expansion by abdominal ascites requiring paracentesis in the delivery room. An echocardiogram on day of life 0 showed a large ventricular septal defect, large patent ductus arteriosus, and high suspicion for coarctation of the aorta. Hemodynamic stability was achieved with the addition of dopamine and hydrocortisone. Although initially presenting with poor perfusion, he later became plethoric, thrombocytopenic, and coagulopathic without active bleeding. He was also noted to have

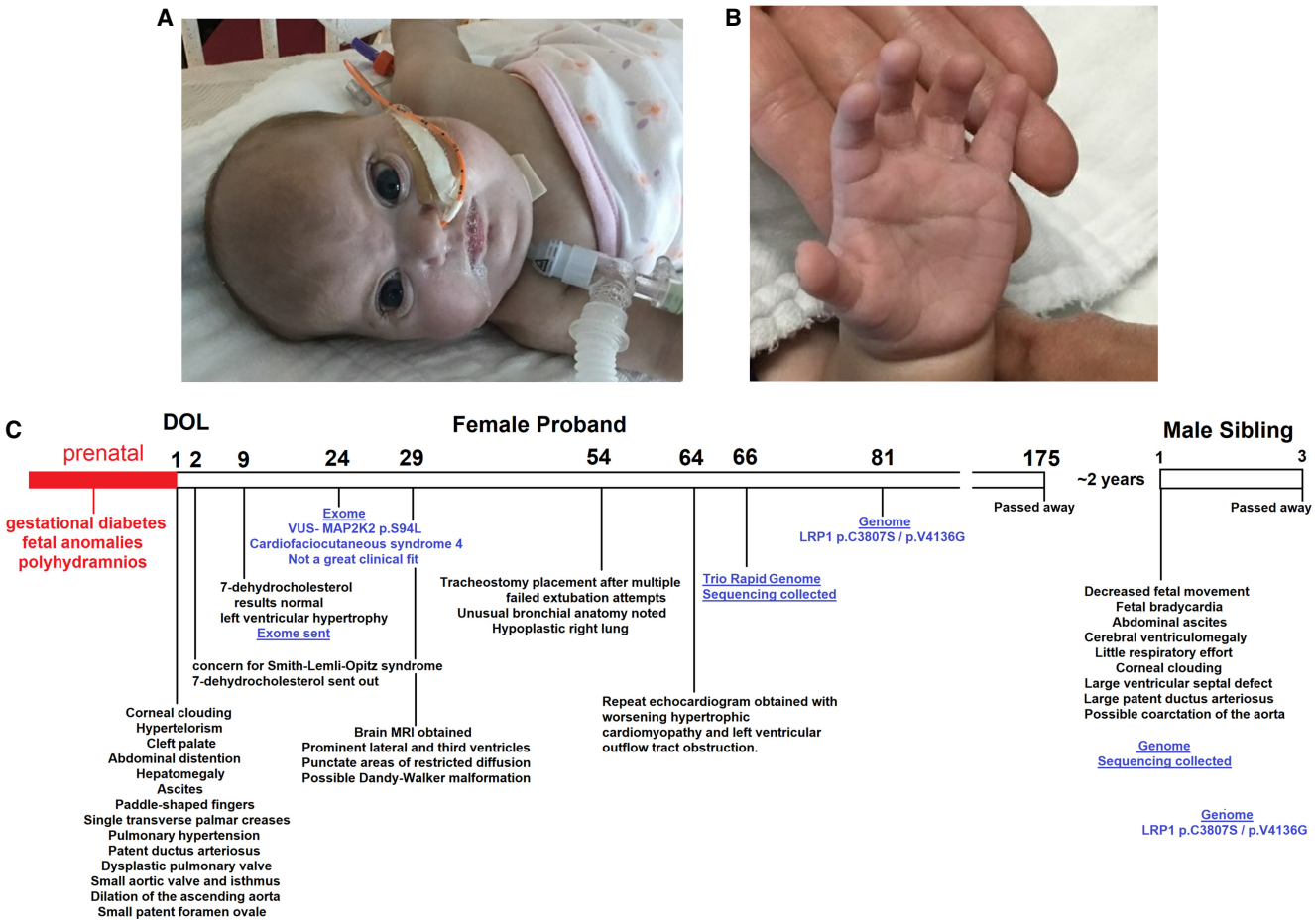

Figure 2. Patient morphology and time line. Facial (*A*) and hand (*B*) morphology of the proband. (*C*) Time line of both probands, including the genomics identified in blue. (DOL) Day of life.

a right-sided closed humeral greenstick fracture without history of birth trauma. Ultrasound revealed bilateral hydronephrosis and proximal hydroureter with grade 3 dilation of the collecting system bilaterally. He remained oliguric. He was profoundly hypotonic and remained mostly unresponsive, with occasional minimal response to painful stimuli. Cranial ultrasound confirmed severe bilateral ventriculomegaly and possible third ventricle dilation. Parents opted for comfort care on day of life 2; he was extubated and expired shortly after. The overlap of phenotypes between the two siblings at various stages is listed in Table 1.

Genome Sequencing

rGS was performed for both children. Blood samples were sent to Rady Children's Institute of Genomic Medicine (RCIGM) for both parents and siblings. Trio-based genome sequence analysis revealed the same compound heterozygous *LRP1* (gene of uncertain significance, GUS) variants in both siblings, classified as VUSs following American College of Medical Genetics and Genomics (ACMG) classification guidelines (Table 2). The first variant, c.11420G > C, (p.Cys3807Ser) was inherited maternally. The second variant, c.12407T > G, (p.Val4136Gly) was inherited paternally. Further analysis of variants between the siblings did not reveal any additional variants that met RCIGM reporting criteria.

Table 1. Overlapping phenotypes between the two siblings

Classification	Phenotypes
Prenatal	Polyhydramnios, cerebral ventriculomegaly, fetal ascites
Facial	Hypertelorism, marked under orbital creases, corneal clouding, large anterior fontanelle, low-set ears
Pulmonary	Severe respiratory distress requiring intubation
Cardiac	Large patent ductus arteriosus, coarctation of the aorta
Abdomen	Profound ascites
Hand and feet	Paddle-shaped fingers and toes
Neurologic	Cerebral ventriculomegaly

LRP1 Variant Analysis

Evolutionary analysis of amino acid conservation (Fig. 3A) and codon selection (Fig. 3B) reveal the majority of LRP1 to be highly conserved, including the regions of the genomic variants p.Cys3807 and p.Val4136 (red lines). The p.Cys3807 amino acid forms a disulfide bond with p.Cys3792 (Fig. 3C) and is conserved throughout LRP1 and the closely related LRP1B (Fig. 3D), highlighting the disulfide bond's importance throughout evolution. The variant p.Cys3807Ser is predicted to be damaging in PolyPhen-2, deleterious in PROVEAN, Class C65 in Align-GVGD, has a codon score of 1.5 (out of 2, with 1.1 standard deviations above the mean of codon selection for any *LRP1* codon), is 100% conserved throughout LRP1 and LRP1B sequences (431 total sequences), and is annotated in UniProt to form a disulfide bond. p.Val4136 is part of a hydrophobic core (Fig. 3C) and is conserved throughout LRP1 and LRP1B (Fig. 3D). The variant p.Val4136Gly is predicted deleterious in PROVEAN, damaging in SIFT, Class C35 in Align-GVGD, under weak selection but with 99% of species for LRP1 conserved as a V, 100% conserved as a hydrophobic amino acid, and has 61% conservation in LRP1B for V. Neither variant has been observed in gnomAD.

As of July 2021, there have been 1978 annotated LRP1 variants from gnomAD, TOPMed, Geno2MP, and ClinVar. Below are several noted variants with relevant connected phenotypes. The homozygous p.Lys1245Arg variant observed in a patient with keratosis pilaris atrophicans (Klar et al. 2015) is conserved as a K in 100% of sequences for LRP1 and LRP1B. It is likely that the Arg at this position does not fully replace Lys, but the functional conservation of the polar basic amino acid maintains most of the protein function to yield a subset of patient phenotypes. Within Geno2MP, an individual homozygous for p.Arg1993Trp is annotated with "abnormality of the cardiovascular system" (HP:0001626) and "abnormality of the cerebral vasculature" (HP:0100659), consistent with the siblings described here. Multiple heterozygous individuals with this same variant have an additional

Table 2. Variant table

Gene	Variant	ClinVar	Zygosity	Variant classification	Inheritance	Patient
LRP1	c.11420G > C, (p.Cys3807Ser)	SCV002569952	Heterozygous	VUS	Maternal	1 and 2
LRP1	c.12407T > G (p.Val4136Gly)	SCV002569951	Heterozygous	VUS	Paternal	1 and 2

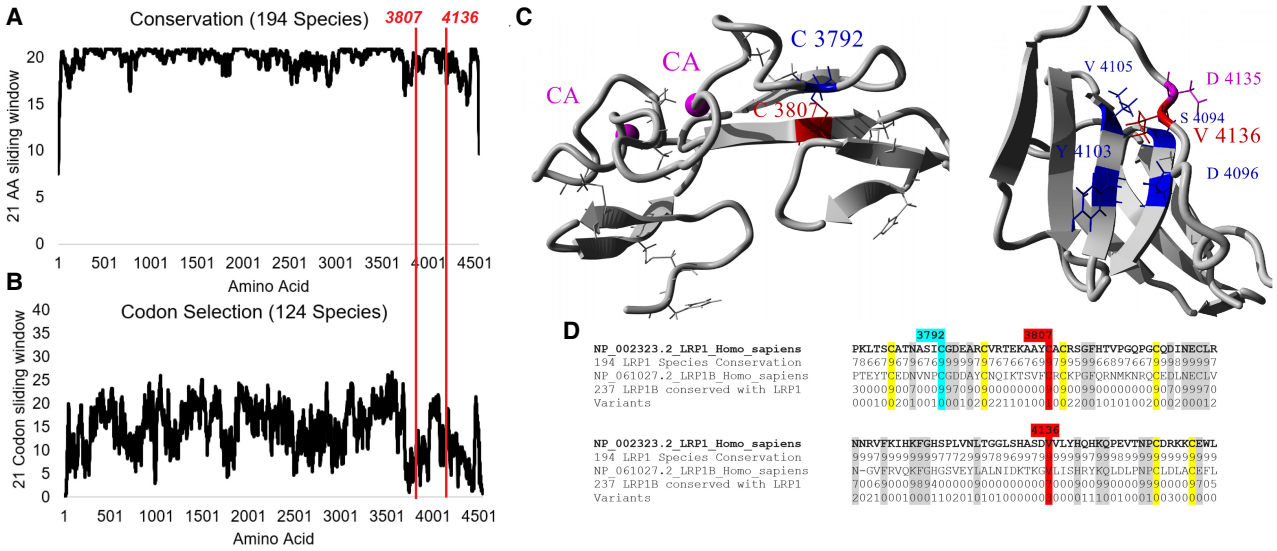

Figure 3. LRP1 variant characterization. Amino acid conservation from 194 LRP1 protein sequences (*A*) or codon selection scores from 124 open reading frame sequences of *LRP1* (*B*). Each is shown as a sliding window of additive conservation of 21 amino acids/codons, and the two variants from patients are marked with a red line. (*C*) Protein models for Cys3807 and Val4136 (red). (*D*) Sequence alignments of LRP1 and LRP1B for amino acids around 3807 and 4136 (red). The 194 protein sequences were determined for conservation of each site (1 to 9, with 9 being >90% conserved), and 237 sequences of LRP1B were used to determine conservation with LRP1 (0 being not conserved with LRP1 and 1 to 9 based on conservation, with 9 being >90% conserved). Cysteines involved in disulfide bonds and conserved are highlighted in yellow, and other amino acids conserved with LRP1B are highlighted in gray.

annotation of "hypoplastic left-heart syndrome" (HP:0004383) and "retinitis pigmentosa" (HP:0000510). Patients with p.Thr780Ile are also enriched for "hypoplastic left-heart syndrome" (HP:0004383). Annotated compound heterozygous damaging variants for LRP1 are observed in ClinVar for one individual (p.Leu526Val/p.Ser4520Cys) with ventricular septal defect and tricuspid atresia (ClinVar VCV000816915/VCV000816916). Two patients with compound heterozygous variants (p.Val315Ala/p.Arg1734His/p.Ser2907Lue/p.Ala3634Thr) from a cardiomyopathy-specific paper by Jin et al. (2017) have also been observed. Additional work needs to be done to compare details of phenotypes within patients with LRP1 variants.

Lrp1 Mouse Phenotypes

Mouse genetic editing can link genes to phenotypes, as assessed for *Lrp1*-related genetic changes (Supplemental Table S1). As part of the Bench to Bassinet Program (Lauer and Skarlatos 2010), chemically induced variants were screened for congenital heart disease. In that work, a homozygous *Lrp1* variant (Lrp1^{b2b1554Clo}, p.Cys4232Arg; http://www.informatics.jax.org/allele/MGI:5437079) was identified to drive embryonic lethality through pulmonary stenosis, atrioventricular septal defect, and pronounced abdominal wall complications. An ENU (*N*-ethyl-*N*-nitrosourea) mutational screen has also identified a craniofacial defect variant in mouse *Lrp1* (c.Thr1019Cys, p.Phe340Ser) that results in abnormal head shape, short snout, smaller size, hemorrhage, body wall abnormalities, altered cleft palate, and short mandible (Fig. 4).

A homozygous knockout of *Lrp1* in mice (replacing the gene with LacZ to track expression, Lrp1$^{tm1.1(KOMP)Wtsi}$) was generated as part of the International Mouse Phenotyping

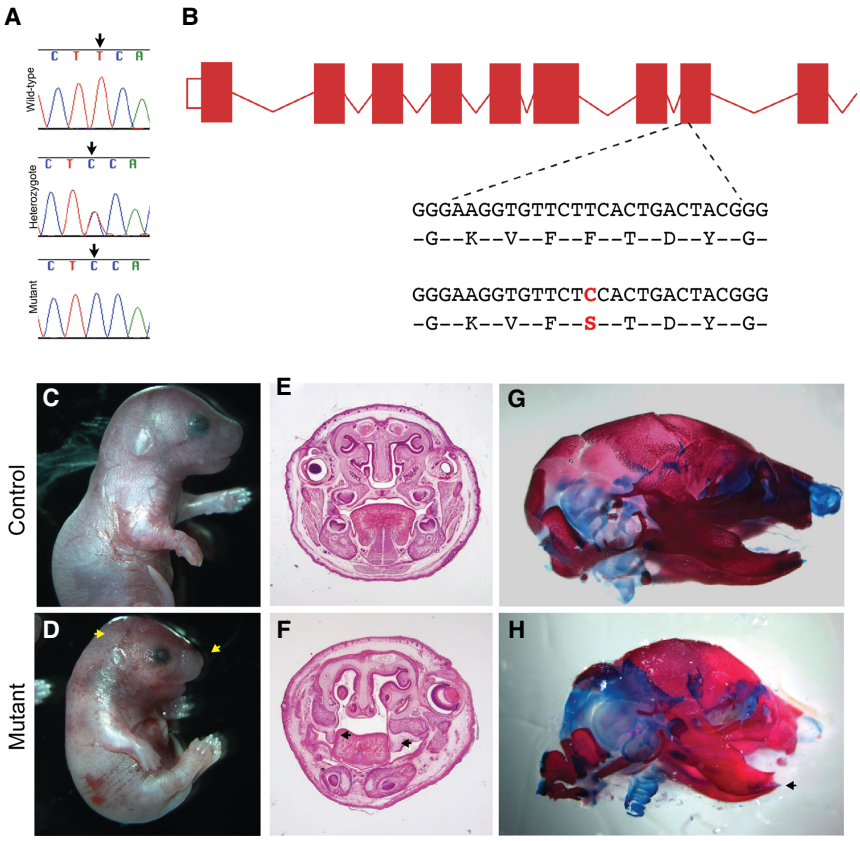

Figure 4. ENU(*N*-ethyl-*N*-nitrosourea) mutation in *Lrp1* results in craniofacial abnormalities in mice. (*A*,*B*) A perinatal recessive ENU screen for novel genes involved craniofacial defects identified a mutant line with a c.Thr1019Cys transition in *Lrp1* resulting in an p.F340S amino acid change, which disrupts the conserved YWTD motif in the extracellular domain. (*C*,*D*) Gross morphology of the ENU mutant, showing an abnormal head shape and short snout (arrow), smaller size, hemorrhage, and body wall abnormalities. (*E*,*F*) Coronal sections of E18.5 mutant and control heads showing cleft secondary palate in mutants. Arrowheads indicate unelevated palate shelves. (*G*,*H*) Alizarin red/alcian blue staining showing overall abnormal skull shape and markedly short mandible (arrow).

Consortium (IMPC) (Meehan et al. 2017). These animals have preweaning lethality, altered heart development, pallor (pigment dysfunction), and abnormal limb morphology (Supplemental Table S2). Staining of embryo shows pronounced expression in bone, head, and abdominal areas (Fig. 5A), which are consistent with parts of our patients' phenotypes.

Three additional homozygous knockout strains ($Lrp1^{tm1Her}$, $Lrp1^{tm3Ajmr}$, $Lrp1^{tm5Ajmn}$) also show embryonic lethality with growth retardation and altered liver morphology (Supplemental Table S1). Heterozygous knockout of *Lrp1* can survive, but show cardiovascular alterations (Supplemental Table S3), heart weight changes (Fig. 5B), and eye dysmorphology (Fig. 5C). The eye changes in IMPC were noted for lens morphology changes in both left and right eyes of at least one male and female, but without complete penetrance and just short of significance (https://www.mousephenotype.org/data/charts?accession=MGI:96828&allele_accession_id=MGI:5494466&zygosity=heterozygote&parameter_stable_id=IMPC_EYE_016_001&pipeline_stable_id=JAX_001&procedure_stable_id=IMPC_EYE_001&parameter_stable_id=IMPC_EYE_016_001). Cardiovascular system dysfunction is the

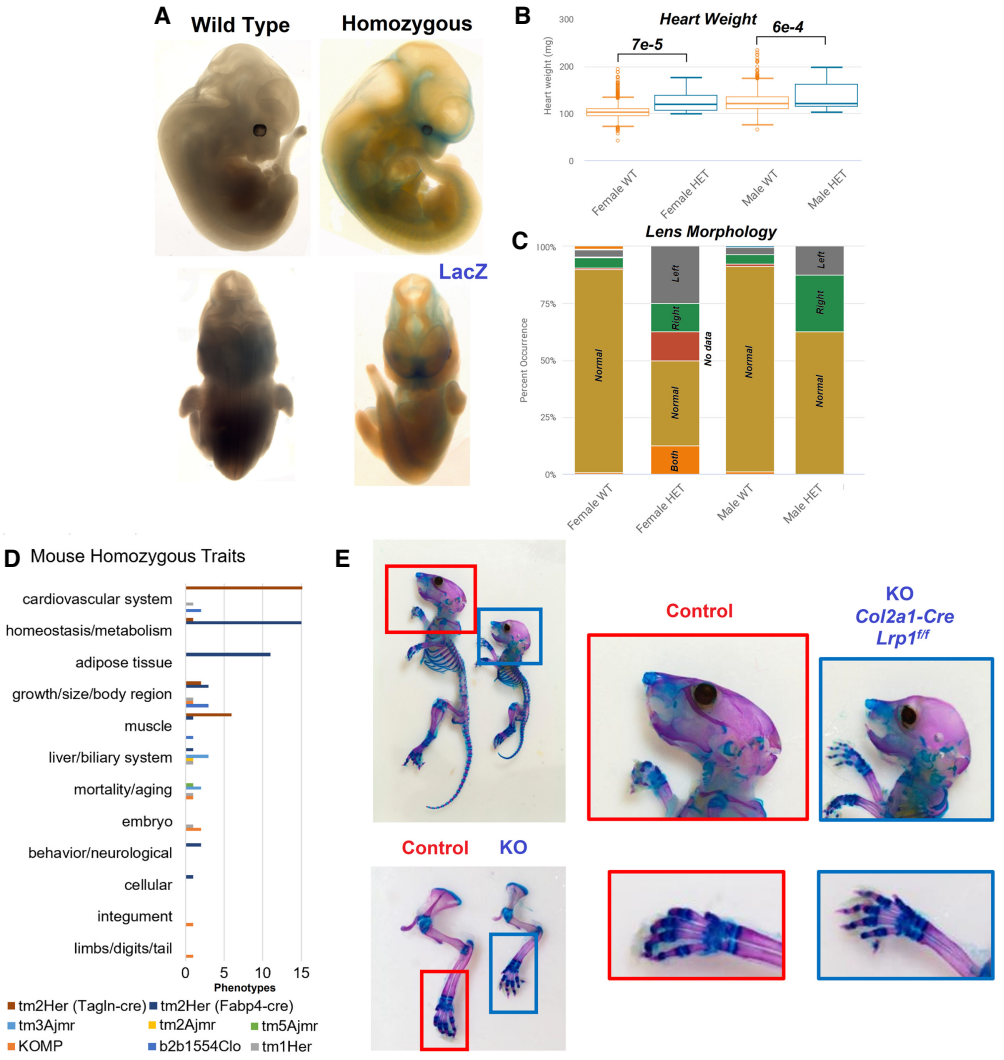

Figure 5. Mouse phenotypes for Lrp1 alterations. (*A*) Embryo imaging of wild-type or *Lrp1* homozygous knockout, with blue representing the LacZ replacement of *Lrp1*. Data is from the International Mouse Phenotyping Consortium (IMPC; www.mousephenotype.org/data/genes/MGI:96828). (*B*,*C*) Heterozygous *Lrp1* knockout causing significant differences in male and female heart weight (*B*) and lens morphology (*C*). (*D*) All phenotypes observed within the Mouse Genome Informatics (MGI) database (Supplemental Table S1) fit within the summary terms for the modified mouse strains. (*E*) Skeleton images of *Col2a1* conditional *Lrp1*-knockout with zoomed images of wild type (red) and homozygous (blue) animals.

most annotated complication of the global and tissue-specific knockout mice generated (Fig. 5D). The Tagln-cre-driven smooth muscle conditional knockout of *Lrp1* shows pronounced alterations of cardiovascular valves and results in dilated cardiomyopathy (Basford et al. 2013). A bone or cartilage conditional knockout for *Lrp1* has been lacking within mouse databases or literature. The Yang lab at Van Andel Institute generated a *Col2a1*-driven *Lrp1* knockout, which results in altered facial morphology and shortened bones, including fingers (Fig. 5E). The mouse phenotypes for *Lrp1* genetic alterations thus provide a remarkable overlap to phenotypes observed within our patients.

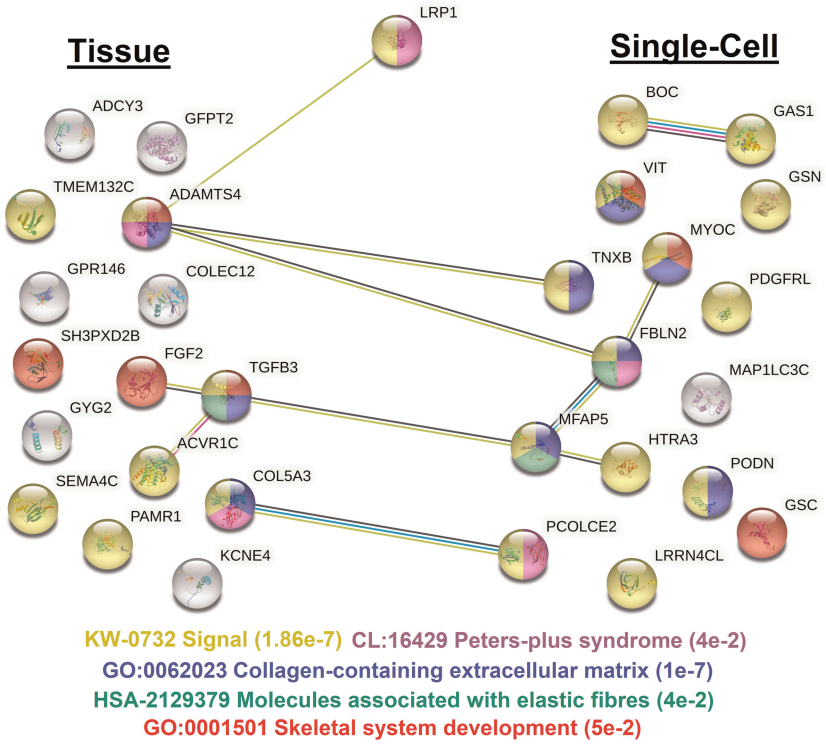

Figure 6. STRING analysis of the top correlating genes based on expression with LRP1. Correlated genes were identified from either human tissue analysis or single-cell analysis. Lines represent known connections from text mining or experimental interactions. The colors of the nodes are based on the phenotypes listed at the bottom, with false discovery rate (FDR) values listed.

LRP1 Human Expression Insights

LRP1 is expressed in most human adult tissues, with high variability, elevation in fibroblasts, and no significant differences between males and females (Supplemental Fig. S2A). Of the 12 known isoforms of the gene, two are found expressed that result in proteins, with the *LRP1-201* isoform (codes for a 4544-amino-acid, full-length protein) found most expressed (Supplemental Fig. S2B). The Human Protein Atlas maintains a list of genes that follow similar correlations to *LRP1* gene expression at the tissue and single-cell levels (Fig. 6; Supplemental Table S4). Analysis of this gene list through OMIM reveals nine genes with known phenotypes, including *SH3PXD2B* with Frank–ter Haar syndrome (dermatocardioskeletal), *MFAP5* with aortic aneurysm, *GSC* with short stature, *TGFB3* with ventricular dysplasia, *MYOC* with glaucoma, *GSN* with amyloidosis, and *TNXB* with Ehlers–Danlos syndrome, classic-like. These phenotypes share some overlap with our patients' features.

The similarly expressed genes are enriched for signaling cascades, specifically collagen-containing extracellular matrix and elastic fibers. In addition, we see genes enriched for skeletal system development and Peters plus syndrome. Peters plus syndrome is an autosomal recessive disorder caused by biallelic variants in *B3GLCT* with pronounced cloudy corneas, clefting, short limb dwarfism, and congenital heart malformation commonly linked to alternating neural crest development (Maillette de Buy Wenniger-Prick and Hennekam 2002), strongly overlapping the individuals described here.

Many of the phenotypes observed within the patients and public data sets, including Peters plus syndrome overlap, involve neural crest cell (NCC)-derived tissues such as vascular smooth muscle and cartilage of heart valves, face, and digits. We utilized transcriptomics of public data sets of NCCs to further our insights. A total of 197 neural crest cell RNA-seq data sets were downloaded from the National Center for Biotechnology Information (NCBI) sequence read archive (SRA) and processed, representing diverse insights from 19 separate studies (Supplemental Fig. S3A). The majority of *LRP1* expression seen from these data sets was from transcript 201 (Supplemental Fig. S3B), representing the full isoform of the LRP1 protein. Few other *LRP* homologous proteins were expressed in the neural crest cells, including no *LRP1B* (Supplemental Fig. S3C). Stratifying expression data sets based on those with >1 standard deviation and those <1 for *LRP1*, 90 genes are higher in *LRP1* enriched data sets and 127 genes lower (Supplemental Fig. S3D). Of these significant genes, there is enrichment for terms (Supplemental Fig. S3D) such as dilated cardiomyopathy (*PCOLCE, COL1A1, TWIST1, SOX9, LOXL1, COL1A2, COL6A2, COL3A1, FBN1, BGN, COL5A1, COL4A1, POSTN, LOXL2*), craniofacial development (*PRRX1, TBX2, TWIST1, SOX9, SIX1, SIX2, ALX1, FOXC2, ALX4, DDR2, ALX3, FOXD3, PRRX2, HES3, MAB21L1, FOXC1, SOX10, SP8*), and blood vessel development (*FAP, COL1A1, PRRX1, TBX2, LRP1, SIX1, PDGFRA, PDGFRB, LOXL1, ACKR3, SFRP2, COL1A2, COL3A1, FOXC2, FN1, COL4A2, COL5A1, COL4A1, FOXC1, LOXL2, GPC3, ACTA2, GPR124, TGFBI, GREM1*).

Human LRP1-Related Phenotypes

The artery and vascular smooth muscle connection of *LRP1* and phenotypes are further supported based on common variants and migraine associations. The variant rs11172113 is the top signal for a significant expression quantitative trait loci (eQTL) of *LRP1* in both aorta and tibial arteries (Supplemental Fig. S4A,B). The peak of the linkage disequilibrium block lies overtop the *LRP1* gene (Supplemental Fig. S4C). Variant rs11172113 is found with a minor allele frequency (MAF) > 0.2 in all gnomAD populations except South Asian, with the highest enrichment in Latino/Admixed Americans (MAF = 0.5). The variant is the lead single-nucleotide polymorphism (SNP) in many migraine, headache, or headache treatment genome/phenome-wide association studies (GWASs/PheWASs; Supplemental Table S5). In most of those studies, this allele has one of the top five significant *P*-values of all sites within the genome. Similar to our patients, this variant is also associated with lung function and artery phenotypes (Supplemental Table S5). There are 33 SNPs with an $R^2 > 0.5$, but only two are >0.8 R^2 (Supplemental Fig. S4D). The lead variant, rs11172113, is located within a highly conserved intronic segment with enhancer annotation and multiple ENCODE-based transcription factor binding events (Supplemental Fig. S5).

Although the effect size in arteries for this allele is small relative to the effect of the missense patient variants, the eQTL and GWASs/PheWASs associations point to similar traits associated with disruption of human *LRP1* as observed in the siblings. These also suggest that some individuals will carry modifying alleles that may result in phenotypic variability because of changes in *LRP1* expression levels that can compensate or exacerbate missense variant associated phenotypes, which requires future analyses.

DISCUSSION

Complete knockout of mouse *Lrp1* results in peri-implantation lethality through dysregulation of the uPA-PAI-1 complex internalization, altering migrating cells (Herz et al. 1992). Mice with a homozygous missense mutation in *Lrp1* at p.Cys4232Arg survive to mid-gestation but die because of cardiac defects (Li et al. 2015). These mice exhibit atrioventricular

septal defects with alteration in outflow tract septation and persistent truncus arteriosus (Lin et al. 2020). The mice die around E14.5–15.5 with 100% penetrant congenital heart defects (Lin et al. 2020). The IMPC's phenotyping of *LRP1* knockout mice reveals homozygous preweaning lethality, altered heart development, pallor (pigment dysfunction), and abnormal limb morphology, with heterozygous knockout mice also having altered cardiovascular and eye phenotypes (Meehan et al. 2017). Additional ENU mutational phenotyping and collagen-specific knockout reveals altered bone and facial development, as shown here for the first time. These phenotypes align with the LRP1-related syndrome of the two individuals described above. Finally, recent work in LRP1 corneal protein interaction networks has shown evidence of the involvement in corneal transparency and structure (Mogensen et al. 2022), supporting our observations.

The missense variant LRP1 protein in cardiac NCCs is retained in the endoplasmic reticulum resulting in decreased cell motility/migration and altered Wnt signaling (Lin et al. 2020). Human *LRP1* is critical for multiple NCC derivatives, including smooth muscle cells (Lehti et al. 2009; Zucker et al. 2019), adipocytes (Masson et al. 2009; Konaniah et al. 2017), chondrocytes (Kawata et al. 2012), osteocytes (Dennis et al. 2020), melanocytes (Cheng et al. 2008), and Schwann cells (Mantuano et al. 2010). Multiple NCC-derived cells have been connected to LRP1 role in amyloid-β uptake and Alzheimer's disease (Kanekiyo et al. 2012; Cheung et al. 2014). *LRP1B* represents the most similar paralog of *LRP1*. Although *LRP1B* is connected to cancer risks (Langbein et al. 2002), it is not redundant with *LRP1*, as shown in the Figure 1 expression, and is not developmentally lethal in knockout mice (Marschang et al. 2004).

Homozygous variants within *LRP1* have been identified as potentially pathogenic for a family with multiple individuals for keratosis pilaris atrophicans based on exome sequencing (Klar et al. 2015). The p.Lys1245Arg variant identified in patients with keratosis pilaris has functional conservation. It does not show the more severe cardiac/bone phenotypes connected to knockout or damaging missense variants of *Lrp1* mouse models, suggesting the change does not reflect a full loss of function within the LRP1 protein like the mouse p.Cys4232Arg or the patients described in this study. Findings within our two siblings presented here build support for cardiac/NCC-derived mouse model findings translating to a human syndrome.

There is ongoing work to identify more patients with *LRP1*-associated variants to define the phenotypic variability, with multiple patients worldwide presenting similar to our patients. Yet, it is already becoming clear from these initial communications and the keratosis pilaris atrophicans patients that there will be broad phenotypic variability for LRP1 variants. We speculate that expression-associated variants such as rs11172113 may likely impact phenotypes when compounded with missense changes. It may be possible that autosomal dominant phenotypes could be observed as homozygous for rs11172113 and having a single heterozygous rare variant. Compound heterozygous changes, such as in our patient, will also likely have more severe phenotypes compounded with heterozygous or homozygous rs11172113 alleles. Further complicating insights for *LRP1* are the many chemicals such as BPA, copper, tobacco, and estradiol that can modulate the expression of *LRP1* (Supplemental Table S6).

This work shows that the human *LRP1* gene variants are associated with pulmonary, cardiac, vascular, and dysmorphic features in an autosomal recessive form similar to the studied mouse models. Subtle *LRP1* eQTLs further support these phenotypes in adult vascular tissues that colocalize with GWASs/PheWASs of vascular dysfunction. Like in the mouse, the human NCCs with elevated *LRP1* have genes highly associated with traits present in the presented siblings. As with nearly all the *LRP*-related genes having human syndromes, we provide the first proof of *LRP1*-associated human autosomal recessive disorder.

METHODS

Sequencing of samples was performed at the CLIA/CAP-certified Rady Children's Institute of Genomic Medicine as previously described (James et al. 2021), with sample collection reviewed and approved by the Spectrum Health or Bronson Institutional Review Board (IRB). The top variants were confirmed with Sanger sequencing. Protein modeling and evolutionary analysis were performed using our published sequence-to-structure-to-function workflow (Prokop et al. 2017). Human variants were extracted on 7/5/2021 for gnomAD (v.2.1.1 nonTOPMed, 135,743 individuals), Bravo (TOPMed; 132,345 individuals), Geno2MP (19,151 individuals), and ClinVar. Mouse phenotypes were extracted from the MGI database (Bult et al. 2008).

Col2a1-Cre and Lrp1 floxed mice were obtained from the Jackson Laboratory and maintained on the C57BL/6 background. The animal maintenance and procedures were approved by the Institutional Animal Care and Use Committee of the Van Andel Research Institute. P14 male mice were used. Skin and internal organs of euthanized mice were removed, and the remaining tissue was fixed in 95% ethanol overnight, followed by incubation in acetone for 24 h. The skeletons were stained with alcian blue (0.015% in 20% acetic acid and 80% ethanol) for 48 h, incubated with 2% KOH for another 48 h, and subsequently stained with alizarin red S (0.005% in 1% KOH) overnight. The stained skeletons were cleared in 1% KOH/20% glycerol solution for 2–3 d and stored in 95% ethanol/glycerol solution (1:1).

Expression analysis of human LRP1 was pulled from GTEx (GTEx Consortium 2020) or Human Protein Atlas (Uhlen et al. 2010). The SRA was searched for "Neural Crest" or "Smooth Muscle," and all deposited human RNA data sets with paired-end, fastq files available, and >10 million matched reads were downloaded with the SRA toolkit. The reads were quasi-aligned to the Gencode38 (Frankish et al. 2019) transcriptome map or RefSeq genes (Prokop et al. 2020) using salmon_0.14.1 (Patro et al. 2017). Mapped transcripts per million (TPM) were processed through NetworkAnalyst3.0 (Zhou et al. 2019) using Limma (Ritchie et al. 2015) statistical analysis of *LRP1* grouped expression. The eQTL data was extracted from GTEx (GTEx Consortium 2020) and assessed using Open Targets Genetics (Ghoussaini et al. 2021), RegulomeDB (Boyle et al. 2012), or the UCSC genome browser (Navarro Gonzalez et al. 2021).

ADDITIONAL INFORMATION

Data Deposition and Access

Raw data for the evolution and all genomic variant analysis can be found at https://doi.org/10.6084/m9.figshare.14920380.v1. Raw data for neural crest RNA-seq can be found at https://doi.org/10.6084/m9.figshare.14920644.v1 and the smooth muscle RNA-seq at https://doi.org/10.6084/m9.figshare.14991444.v1. All images are available in high resolution at https://doi.org/10.6084/m9.figshare.20510904.v1. Interpreted variants have been submitted to ClinVar (https://www.ncbi.nlm.nih.gov/clinvar/) and can be found under accession numbers SCV002569951 and SCV002569952.

Ethics Statement

Patients were consented according to approved protocols reviewed by Spectrum Health and Bronson IRBs. Sequencing was performed according to approved IRB at Rady Children's Institute of Genomics Medicine. All animal work was approved by the Institutional Animal Care and Use Committee (IACUC) at either the Jackson Laboratory or Van Andel Institute.

Competing Interest Statement

The authors have declared no competing interest.

Referees

Lance P. Doucette
Anonymous

Received November 29, 2021; accepted in revised form August 22, 2022.

Author Contributions

P.R.M., C.P.B., and J.W.P. designed and oversaw experiments. P.R.M., A.E., D.L., J.Z., L.Z.R., S.R., and J.W.P contributed to interpretation of data. P.R.M. and A.L. treated patients and formed clinical descriptions. L.G., K.W., and M.S.W. analyzed rapid genome sequencing. S.A.M., T.Y., and D.L. generated or analyzed mouse data. P.R.M., A.E., and J.W.P. generated figures and wrote the manuscript. All authors approved of the final manuscript.

Funding

This work was supported by the Helen DeVos Children's Hospital Foundation, Gerber Foundation, National Institutes of Health (K01ES025435 to J.W.P.), and Michigan State University.

REFERENCES

Basford JE, Koch S, Anjak A, Singh VP, Krause EG, Robbins N, Weintraub NL, Hui DY, Rubinstein J. 2013. Smooth muscle LDL receptor-related protein-1 deletion induces aortic insufficiency and promotes vascular cardiomyopathy in mice. *PLoS ONE* **8:** e82026. doi:10.1371/journal.pone.0082026

Beuschel J, Geyer H, Rich M, Leimanis M, Kampfschulte A, VanSickle E, Rajasekaran S, Bupp C. 2021. Leveraging rapid genome sequencing to alter care plans for pediatric patients in a community hospital setting in the United States. *J Pediatr* **239:** 235–239. doi:10.1016/j.jpeds.2021.08.010

Bick D, Fraser PC, Gutzeit MF, Harris JM, Hambuch TM, Helbling DC, Jacob HJ, Kersten JN, Leuthner SR, May T, et al. 2017. Successful application of whole genome sequencing in a medical genetics clinic. *J Pediatr Genet* **6:** 61–76.

Boyle AP, Hong EL, Hariharan M, Cheng Y, Schaub MA, Kasowski M, Karczewski KJ, Park J, Hitz BC, Weng S, et al. 2012. Annotation of functional variation in personal genomes using RegulomeDB. *Genome Res* **22:** 1790–1797. doi:10.1101/gr.137323.112

Bult CJ, Eppig JT, Kadin JA, Richardson JE, Blake JA, Mouse Genome Database Group. 2008. The Mouse Genome Database (MGD): mouse biology and model systems. *Nucl Acids Res* **36:** D724–D728. doi:10.1093/nar/gkm961

Cadigan KM, Liu YI. 2006. Wnt signaling: complexity at the surface. *J Cell Sci* **119:** 395–402. doi:10.1242/jcs.02826

Cheng C-F, Fan J, Fedesco M, Guan S, Li Y, Bandyopadhyay B, Bright AM, Yerushalmi D, Liang M, Chen M, et al. 2008. Transforming growth factor α (TGFα)-stimulated secretion of HSP90α: using the receptor LRP-1/CD91 to promote human skin cell migration against a TGFβ-rich environment during wound healing. *Mol Cell Biol* **28:** 3344–3358. doi:10.1128/MCB.01287-07

Cheung C, Goh YT, Zhang J, Wu C, Guccione E. 2014. Modeling cerebrovascular pathophysiology in amyloid-β metabolism using neural-crest-derived smooth muscle cells. *Cell Rep* **9:** 391–401. doi:10.1016/j.celrep.2014.08.065

Cong F, Schweizer L, Varmus H. 2004. Wnt signals across the plasma membrane to activate the β-catenin pathway by forming oligomers containing its receptors, Frizzled and LRP. *Development* **131:** 5103–5115. doi:10.1242/dev.01318

Dennis EP, Edwards SM, Jackson RM, Hartley CL, Tsompani D, Capulli M, Teti A, Boot-Handford RP, Young DA, Piróg KA, et al. 2020. CRELD2 is a novel LRP1 chaperone that regulates noncanonical WNT signaling in skeletal development. *J Bone Miner Res* **35:** 1452–1469. doi:10.1002/jbmr.4010

Donnai D, Barrow M. 1993. Diaphragmatic hernia, exomphalos, absent corpus callosum, hypertelorism, myopia, and sensorineural deafness: a newly recognized autosomal recessive disorder? *Am J Med Genet* **47:** 679–682. doi:10.1002/ajmg.1320470518

Farnaes L, Hildreth A, Sweeney NM, Clark MM, Chowdhury S, Nahas S, Cakici JA, Benson W, Kaplan RH, Kronick R, et al. 2018. Rapid whole-genome sequencing decreases infant morbidity and cost of hospitalization. *NPJ Genomic Med* **3:** 10. doi:10.1038/s41525-018-0049-4

Frankish A, Diekhans M, Ferreira A-M, Johnson R, Jungreis I, Loveland J, Mudge JM, Sisu C, Wright J, Armstrong J, et al. 2019. GENCODE reference annotation for the human and mouse genomes. *Nucl Acids Res* **47:** D766–D773. doi:10.1093/nar/gky955

Ghoussaini M, Mountjoy E, Carmona M, Peat G, Schmidt EM, Hercules A, Fumis L, Miranda A, Carvalho-Silva D, Buniello A, et al. 2021. Open Targets Genetics: systematic identification of trait-associated genes using

large-scale genetics and functional genomics. *Nucl Acids Res* **49:** D1311–D1320. doi:10.1093/nar/gkaa840

Gong Y, Slee RB, Fukai N, Rawadi G, Roman-Roman S, Reginato AM, Wang H, Cundy T, Glorieux FH, Lev D, et al. 2001. LDL receptor-related protein 5 (LRP5) affects bone accrual and eye development. *Cell* **107:** 513–523. doi:10.1016/S0092-8674(01)00571-2

GTEx Consortium. 2020. The GTEx Consortium atlas of genetic regulatory effects across human tissues. *Science* **369:** 1318–1330. doi:10.1126/science.aaz1776

Herz J, Clouthier DE, Hammer RE. 1992. LDL receptor-related protein internalizes and degrades uPA-PAI-1 complexes and is essential for embryo implantation. *Cell* **71:** 411–421. doi:10.1016/0092-8674(92)90511-A

James KN, Lau M, Shayan K, Lenberg J, Mardach R, Ignacio R, Halbach J, Choi L, Kumar S, Ellsworth KA. 2021. Expanding the genotypic spectrum of *ACTG2*-related visceral myopathy. *Cold Spring Harb Mol Case Stud* **7:** a006085. doi:10.1101/mcs.a006085

Jin SC, Homsy J, Zaidi S, Lu Q, Morton S, DePalma SR, Zeng X, Qi H, Chang W, Sierant MC, et al. 2017. Contribution of rare inherited and de novo variants in 2,871 congenital heart disease probands. *Nat Genet* **49:** 1593–1601. doi:10.1038/ng.3970

Kanekiyo T, Liu C-C, Shinohara M, Li J, Bu G. 2012. LRP1 in brain vascular smooth muscle cells mediates local clearance of Alzheimer's amyloid-β. *J Neurosci* **32:** 16458–16465. doi:10.1523/JNEUROSCI.3987-12.2012

Kawata K, Kubota S, Eguchi T, Aoyama E, Moritani NH, Kondo S, Nishida T, Takigawa M. 2012. Role of LRP1 in transport of CCN2 protein in chondrocytes. *J Cell Sci* **125:** 2965–2972.

Klar J, Schuster J, Khan TN, Jameel M, Mäbert K, Forsberg L, Baig SA, Baig SM, Dahl N. 2015. Whole exome sequencing identifies *LRP1* as a pathogenic gene in autosomal recessive keratosis pilaris atrophicans. *J Med Genet* **52:** 599–606. doi:10.1136/jmedgenet-2014-102931

Konaniah ES, Kuhel DG, Basford JE, Weintraub NL, Hui DY. 2017. Deficiency of LRP1 in mature adipocytes promotes diet-induced inflammation and atherosclerosis-brief report. *Arterioscler Thromb Vasc Biol* **37:** 1046–1049. doi:10.1161/ATVBAHA.117.309414

Langbein S, Szakacs O, Wilhelm M, Sukosd F, Weber S, Jauch A, Lopez Beltran A, Alken P, Kälble T, Kovacs G. 2002. Alteration of the *LRP1B* gene region is associated with high grade of urothelial cancer. *Lab Investig J Tech Methods Pathol* **82:** 639–643. doi:10.1038/labinvest.3780458

Lauer MS, Skarlatos S. 2010. Translational research for cardiovascular diseases at the National Heart, Lung, and Blood Institute: moving from bench to bedside and from bedside to community. *Circulation* **121:** 929–933. doi:10.1161/CIRCULATIONAHA.109.917948

Lehti K, Rose NF, Valavaara S, Weiss SJ, Keski-Oja J. 2009. MT1-MMP promotes vascular smooth muscle dedifferentiation through LRP1 processing. *J Cell Sci* **122:** 126–135. doi:10.1242/jcs.035279

Li Y, Pawlik B, Elcioglu N, Aglan M, Kayserili H, Yigit G, Percin F, Goodman F, Nürnberg G, Cenani A, et al. 2010. LRP4 mutations alter Wnt/β-catenin signaling and cause limb and kidney malformations in Cenani–Lenz syndrome. *Am J Hum Genet* **86:** 696–706. doi:10.1016/j.ajhg.2010.03.004

Li Y, Klena NT, Gabriel GC, Liu X, Kim AJ, Lemke K, Chen Y, Chatterjee B, Devine W, Damerla RR, et al. 2015. Global genetic analysis in mice unveils central role for cilia in congenital heart disease. *Nature* **521:** 520–524. doi:10.1038/nature14269

Lin J-HI, Feinstein TN, Jha A, McCleary JT, Xu J, Arrigo AB, Rong G, Maclay LM, Ridge T, Xu X, et al. 2020. Mutation of LRP1 in cardiac neural crest cells causes congenital heart defects by perturbing outflow lengthening. *Commun Biol* **3:** 312. doi:10.1038/s42003-020-1035-9

Maillette de Buy Wenniger-Prick LJ, Hennekam RC. 2002. The Peters' plus syndrome: a review. *Ann Genet* **45:** 97–103. doi:10.1016/S0003-3995(02)01120-6

Mantuano E, Jo M, Gonias SL, Campana WM. 2010. Low density lipoprotein receptor-related protein (LRP1) regulates Rac1 and RhoA reciprocally to control Schwann cell adhesion and migration. *J Biol Chem* **285:** 14259–14266. doi:10.1074/jbc.M109.085126

Marschang P, Brich J, Weeber EJ, Sweatt JD, Shelton JM, Richardson JA, Hammer RE, Herz J. 2004. Normal development and fertility of knockout mice lacking the tumor suppressor gene *LRP1b* suggest functional compensation by *LRP1*. *Mol Cell Biol* **24:** 3782–3793. doi:10.1128/MCB.24.9.3782-3793.2004

Masson O, Chavey C, Dray C, Meulle A, Daviaud D, Quilliot D, Muller C, Valet P, Liaudet-Coopman E. 2009. LRP1 receptor controls adipogenesis and is up-regulated in human and mouse obese adipose tissue. *PLoS ONE* **4:** e7422. doi:10.1371/journal.pone.0007422

Meehan TF, Conte N, West DB, Jacobsen JO, Mason J, Warren J, Chen C-K, Tudose I, Relac M, Matthews P, et al. 2017. Disease model discovery from 3,328 gene knockouts by the International Mouse Phenotyping Consortium. *Nat Genet* **49:** 1231–1238. doi:10.1038/ng.3901

Mogensen EH, Poulsen ET, Thøgersen IB, Yamamoto K, Brüel A, Enghild JJ. 2022. The low-density lipoprotein receptor-related protein 1 (LRP1) interactome in the human cornea. *Exp Eye Res* **219:** 109081. doi:10.1016/j.exer.2022.109081

Navarro Gonzalez J, Zweig AS, Speir ML, Schmelter D, Rosenbloom KR, Raney BJ, Powell CC, Nassar LR, Maulding ND, Lee CM, et al. 2021. The UCSC Genome Browser database: 2021 update. *Nucl Acids Res* **49:** D1046–D1057. doi:10.1093/nar/gkaa1070

Owen MJ, Niemi A-K, Dimmock DP, Speziale M, Nespeca M, Chau KK, Van Der Kraan L, Wright MS, Hansen C, Veeraraghavan N, et al. 2021. Rapid sequencing-based diagnosis of thiamine metabolism dysfunction syndrome. *N Engl J Med* **384:** 2159–2161. doi:10.1056/NEJMc2100365

Patro R, Duggal G, Love MI, Irizarry RA, Kingsford C. 2017. Salmon provides fast and bias-aware quantification of transcript expression. *Nat Methods* **14:** 417–419. doi:10.1038/nmeth.4197

Prokop JW, Lazar J, Crapitto G, Smith DC, Worthey EA, Jacob HJ. 2017. Molecular modeling in the age of clinical genomics, the enterprise of the next generation. *J Mol Model* **23:** 75. doi:10.1007/s00894-017-3258-3

Prokop JW, May T, Strong K, Bilinovich SM, Bupp C, Rajasekaran S, Worthey EA, Lazar J. 2018. Genome sequencing in the clinic: the past, present, and future of genomic medicine. *Physiol Genomics* **50:** 563–579. doi:10.1152/physiolgenomics.00046.2018

Prokop JW, Shankar R, Gupta R, Leimanis ML, Nedveck D, Uhl K, Chen B, Hartog NL, Van Veen J, Sisco JS, et al. 2020. Virus-induced genetics revealed by multidimensional precision medicine transcriptional workflow applicable to COVID-19. *Physiol Genomics* **52:** 255–268. doi:10.1152/physiolgenomics.00045.2020

Ritchie ME, Phipson B, Wu D, Hu Y, Law CW, Shi W, Smyth GK. 2015. limma powers differential expression analyses for RNA-sequencing and microarray studies. *Nucl Acids Res* **43:** e47. doi:10.1093/nar/gkv007

Terrand J, Bruban V, Zhou L, Gong W, El Asmar Z, May P, Zurhove K, Haffner P, Philippe C, Woldt E, et al. 2009. LRP1 controls intracellular cholesterol storage and fatty acid synthesis through modulation of Wnt signaling. *J Biol Chem* **284:** 381–388. doi:10.1074/jbc.M806538200

Uhlen M, Oksvold P, Fagerberg L, Lundberg E, Jonasson K, Forsberg M, Zwahlen M, Kampf C, Wester K, Hober S, et al. 2010. Towards a knowledge-based Human Protein Atlas. *Nat Biotechnol* **28:** 1248–1250. doi:10.1038/nbt1210-1248

Zhou G, Soufan O, Ewald J, Hancock REW, Basu N, Xia J. 2019. NetworkAnalyst 3.0: a visual analytics platform for comprehensive gene expression profiling and meta-analysis. *Nucl Acids Res* **47:** W234–W241. doi:10.1093/nar/gkz240

Zucker MM, Wujak L, Gungl A, Didiasova M, Kosanovic D, Petrovic A, Klepetko W, Schermuly RT, Kwapiszewska G, Schaefer L, et al. 2019. LRP1 promotes synthetic phenotype of pulmonary artery smooth muscle cells in pulmonary hypertension. *Biochim Biophys Acta Mol Basis Dis* **1865:** 1604–1616. doi:10.1016/j.bbadis.2019.03.012